Generation of bipedal walking through interactions among the robot dynamics, the oscillator dynamics, and the environment: Stability characteristics of a five-link planar biped robot

Shinya Aoi and Kazuo Tsuchiya

Abstract We previously developed a locomotion control system for a biped robot using nonlinear oscillators and verified the performance of this system in order to establish adaptive walking through the interactions among the robot dynamics, the oscillator dynamics, and the environment. In order to clarify these mechanisms, we investigate the stability characteristics of walking using a five-link planar biped robot with a torso and knee joints that has an internal oscillator with a stable limit cycle to generate the joint motions. Herein we conduct numerical simulations and a stability analysis, where we analytically obtain approximate periodic solutions and examine local stability using a Poincaré map. These analyses reveal 1) stability characteristics due to locomotion speed, torso, and knee motion, 2) stability improvement due to the modulation of oscillator states based on phase resetting using foot-contact information, and 3) the optimal parameter in the oscillator dynamics for adequately exploiting the interactions among the robot dynamics, the oscillator dynamics, and the environment in order to increase walking stability. The results of the present study demonstrate the advantage and usefulness of locomotion control using oscillators through mutual interactions.

Keywords Biped robot · Oscillator · Central pattern generator · Phase resetting · Stability analysis · Poincaré map · Optimization

Shinya Aoi
Dept. of Aeronautics and Astronautics, Graduate School of Engineering, Kyoto University
Yoshida-honmachi, Sakyo-ku, Kyoto 606-8501, Japan
Tel.: +81-75-753-5809
Fax: +81-75-753-5809
E-mail: shinya_aoi@kuaero.kyoto-u.ac.jp

Kazuo Tsuchiya
Dept. of Energy and Mechanical Engineering, Faculty of Science and Engineering, Doshisha University
1-3 Tatara, Miyakodani, Kyotanabe, Kyoto 610-0394, Japan

Shinya Aoi and Kazuo Tsuchiya
JST, CREST, 5 Sanbancho, Chiyoda-ku, Tokyo 102-0075, Japan

1 Introduction

A number of studies have developed sophisticated biped robots and have successfully established bipedal walking based on model-based approaches using inverse kinematics and kinetics [25,31,35,38,42,60], which basically generate robot motions based on criteria such as the zero moment point [56]. However, accurate modeling of both the robot and the environment and complicated computations are necessary. The difficulty of achieving adaptability to various environments in the real world is often cited to illustrate this point. Designing a locomotion control system to obtain such adaptability is crucial.

In contrast to robots, animals generate locomotion that is adaptive to diverse environments by cooperatively manipulating their complicated and redundant musculoskeletal systems, where the most crucial considerations are muscle tone control and rhythm control. A number of studies on robotics have been inspired by biological and physiological findings and have achieved adaptive walking. Actually, a number of researchers have demonstrated the essential role of muscle tone control by appropriately applying mechanical compliance in hexapod [1,7,12,46,49], quadruped [19,33,45], and biped robots [26,54,59]. On the other hand, we focused on the rhythm control [2,3] inspired by central pattern generators (CPGs) [22,23,43], which generate rhythmic motor patterns in the spinal cord

to create limb movements in animal walking. Central pattern generators modulate rhythmic patterns in response to sensory information, resulting in adaptive behaviors. Central pattern generators are widely modeled using nonlinear oscillators [28, 51–53], and based on such CPG models, a number of walking robots and their control systems have been developed, in particular, for quadruped robots [19, 33, 36, 55], multi-legged robots [29, 62], snake-like and salamander robots [27, 28, 30], and biped robots [37, 40, 47].

In previous studies, we developed a locomotion control system for a biped robot by referring to CPG characteristics [2, 3]. In this system, the control system consisted of internal oscillators that have their own dynamics with a stable limit cycle. The oscillators generated desired robot motions, and the oscillator states were modulated by phase resetting based on foot-contact information, meaning that the walking behavior is generated through the interactions among the robot dynamics, the oscillator dynamics, and the environment. Although we only used joint and foot-contact information without using information regarding ground reaction forces or the absolute orientation of the robot relative to the ground, we accomplished adaptive bipedal walking. For example, the gait cycle was modulated depending on the environmental situation, such as the slope angle [2], and the phase difference of the leg movements between the right and left legs was modulated during turning [3], as in human walking [16]. The proposed control system did not require accurate modeling or complicated calculations. Although the control scheme was simple, such obtained adaptabilities were notable.

The performance of the proposed control system was verified by numerical simulations and hardware experiments [2, 3]. However, the mechanisms for achieving adaptive walking through the dynamic interactions among the robot, the oscillators, and the environments were not necessarily clear. Therefore, we analytically investigated these mechanisms based on a simple compass model composed of three point masses, revealing the self-stability characteristics [4], period-doubling bifurcations, and chaotic behaviors [5], and the stability improvement due to phase resetting using the foot-contact information [6]. However, the compass model is very restricted and does not represent actual biped robots. Actual robots have a torso, with the center of mass located above the hip joints, and knee joints, that generate clearance to prevent the swing leg from scraping the ground. The influence of these considerations on the generation of walking behavior must be clarified in order to completely understand the mechanisms by which to create adaptive walking.

Although the interactions among the robot dynamics, the oscillator dynamics, and the environment are crucial for generating walking, there is no guiding principle for designing these interactions. The proposed control system produced such interactions by the modulation of the oscillator states based on phase resetting using crucial foot-contact information. However, it is generally difficult to determine the parameters in the control system to generate adequate interactions to create adaptive walking.

To clarify the issues surrounding adaptive walking, in the present paper, we used a five-link planar biped robot with a torso and knee joints that has an internal oscillator with a stable limit cycle to generate joint motions. We investigated walking behavior through numerical simulations and stability analysis in which we analytically obtained approximate periodic solutions and examined local stability using a Poincaré map. These analyses reveal 1) stability characteristics due to locomotion speed, torso, and knee motion, 2) stability improvement due to the modulation of oscillator states based on phase resetting using foot-contact information, and 3) the optimal parameter in the oscillator dynamics for adequately exploiting the interactions among the robot dynamics, the oscillator dynamics, and the environment in order to increase walking stability.

The remainder of the present paper is organized as follows. Section 2 introduces the five-link planar biped robot model and demonstrates walking behavior driven by an internal oscillator. Section 3 investigates the stability characteristics of the walking behavior, and Section 4 verifies the stability improvement by modulating walking behavior through phase resetting using foot-contact information and deals with the parameter optimization. Sections 5 and 6 present a discussion and the conclusions, respectively.

2 Model and walking behavior driven by an internal oscillator

2.1 Biped robot model

Figure 1 shows a schematic model of a biped robot comprised of a torso and two legs. Each leg consists of two links (femur and tibia). The model walks on flat ground and is constrained on the x-y plane, where the walking direction is along the x-axis. When the stance leg is in contact with the ground, the tip of the stance leg is constrained on the ground without slipping. The model has a touch sensor attached to the tip of each leg and proprioceptive sensors to monitor the joint angles of the leg. All joints have motors to manipulate the angles. The model, however, has no actuator between the
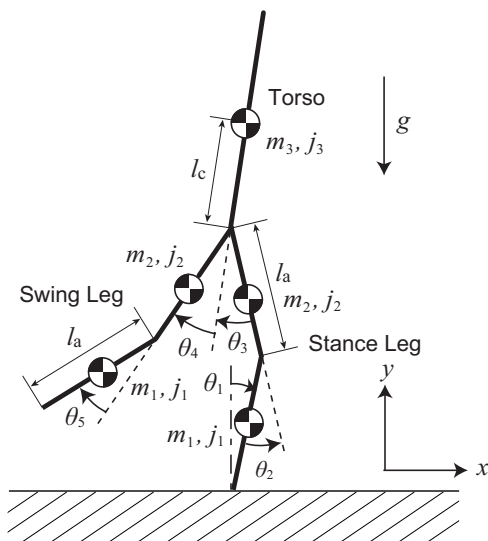
Fig. 1 Schematic diagram of the five-link planar biped robot

tips of the legs and the ground. In addition, the model has no sensor to directly monitor its posture, i.e., the absolute orientation of the robot with respect to the ground. Therefore, it is necessary to establish adequate postural behavior in order to generate stable walking by controlling the internal joints of the robot based on such local information as joint states and intermittent foot-contact information.

The lengths of the femur and tibia are both l_a. The centers of mass of the femur and tibia are located at the center of each link. The legs are connected to the torso at the hips at a distant of l_c from the center of the mass of the torso. The masses of the tibia, femur, and torso are m_1, m_2, and m_3, respectively. The moments of inertia around the center of mass of the tibia, femur, and torso are j_1, j_2, and j_3, respectively. Acceleration due to gravity is g.

We introduce relative angle θ_i $(i = 1, \ldots, 5)$ to describe the configuration of the robot model. Angle θ_1 is the angle of the tibia of the stance leg relative to a line perpendicular to the ground, which corresponds to the posture angle (absolute orientation of the robot) with respect to the ground. Angles θ_2, θ_3, θ_4, and θ_5 are relative angles between the tibia and femur of the stance leg, between the femur of the stance leg and the torso, between the torso and the femur of the swing leg, and between the femur and tibia of the swing leg, respectively. Since each joint has a motor to control its behavior, except for angle θ_1, joint angles θ_i $(i = 2, \ldots, 5)$ are directly manipulated by the motors.

The step cycle of the walking motion consists of two types of successive phases: swing and foot contact

phases. In the following sections, we explain the governing equations for these phases.

2.2 Swing phase model

When the model is supported only by the stance leg and the swing leg is not in contact with the ground, the equation of motion for state variable $q^T = [\theta_1\,\theta_2\,\theta_3\,\theta_4\,\theta_5] \in \mathbb{R}^5$ is given as

$$K(q)\ddot{q} + c(q,\dot{q}) + \nu(q) = u(q,\dot{q}) \tag{1}$$

where $K(q) \in \mathbb{R}^{5\times5}$ is the inertia matrix, $c(q,\dot{q}) \in \mathbb{R}^5$ is the nonlinear term, $\nu(q) \in \mathbb{R}^5$ is the gravity term, and $u(q,\dot{q}) \in \mathbb{R}^5$ is the input torque term (see Appendix A).

The model receives reaction force $\lambda^T = [\lambda_x\,\lambda_y]$ from the ground, where λ_x and λ_y represent the horizontal and vertical components, respectively. This force, which is equivalent to the constrained force to kinematically fix the tip of the stance leg on the ground, can be derived from the equation of motion using generalized state variables, including the position of the tip of the stance leg relative to the ground (see Appendix A). When the reaction force satisfies the condition whereby $|\lambda_x| < \mu|\lambda_y|$ during this phase, where μ is the static friction coefficient, the tip of the stance leg remains constrained on the ground. Otherwise, the tip of the stance leg slips relative to the ground, which destroys the physical conditions for investigating walking behavior. Therefore, the condition of the tip of the stance leg must be verified in order to validate the investigation of the walking motion of the model, which is discussed in Section 2.5.

The motors manipulate the joints based on PD feedback control using the desired states. Letting input torque term $u(q,\dot{q})^T = [0\,u_2\,\ldots\,u_5]$, input torque u_i $(i = 2, \ldots, 5)$ of each motor is given by

$$u_i = -\kappa_i(\theta_i - \hat{\theta}_i) - \sigma_i(\dot{\theta}_i - \dot{\hat{\theta}}_i) \quad i = 2, \ldots, 5 \tag{2}$$

where κ_i and σ_i $(i = 2, \ldots, 5)$ are the gain constants and $\hat{\theta}_i$ and $\dot{\hat{\theta}}_i$ $(i = 2, \ldots, 5)$ are the desired states of θ_i and $\dot{\theta}_i$, respectively, as explained in Section 2.4.

2.3 Foot contact model

When the tip of the swing leg touches the ground, both legs contact the ground. During such a double-supported phase, the model receives two reaction forces from the ground. In general, humans and biped robots have a step cycle of approximately 10% for the double-supported phase during walking. As walking speed increases, the ratio of the double-supported phase decreases. In the foot contact model, we follow the as-

sumptions given in [24] and concentrate on the condition in which the swing leg has no slip and no rebound at the foot contact and the double-supported phase duration is sufficiently short relative to the step cycle. This implies that immediately following the foot contact of the swing leg, the tip of the swing leg is in turn constrained on the ground and the stance leg leaves the ground, i.e., the swing leg instantaneously becomes the stance leg, and vice versa.

The geometric condition for the swing leg to touch the ground is given by

$$r(q) = \cos\theta_1 + \cos(\theta_1 + \theta_2) - \cos(\theta_1 + \theta_2 + \theta_3 + \theta_4)$$
$$- \cos(\theta_1 + \theta_2 + \theta_3 + \theta_4 + \theta_5) = 0 \qquad (3)$$

Since the roles of the legs switch between swing and stance immediately following foot contact, the relationship of the angles between just before and after foot contact is obtained by

$$\begin{bmatrix} \theta_1^+ \\ \theta_2^+ \\ \theta_3^+ \\ \theta_4^+ \\ \theta_5^+ \end{bmatrix} = \begin{bmatrix} 1 & 1 & 1 & 1 & 1 \\ 0 & 0 & 0 & 0 & -1 \\ 0 & 0 & 0 & -1 & 0 \\ 0 & 0 & -1 & 0 & 0 \\ 0 & -1 & 0 & 0 & 0 \end{bmatrix} \begin{bmatrix} \theta_1^- \\ \theta_2^- \\ \theta_3^- \\ \theta_4^- \\ \theta_5^- \end{bmatrix} \qquad (4)$$

where $()^-$ and $()^+$ indicate the state immediately before and after foot contact, respectively. We write this equation as $q^+ = S_c q^-$.

When the tip of the swing leg touches the ground, the leg tip receives an impact from the ground and the angular velocities suddenly change. Following [24], we assume that the stance leg lifts off the ground without interaction and that the double-supported phase duration is infinitesimally small relative to the time constant of the feedback control of the motors. Angular velocity $\dot{q}^+$ immediately after the foot contact and impulse $\xi^{\mathrm{T}} = [\,\xi_x\ \xi_y\,]$ of this foot contact are given as (see Appendix A)

$$\dot{q}^+ = Q(q^-)\dot{q}^- \qquad (5)$$
$$\xi = X(q^-)\dot{q}^- \qquad (6)$$

Note that, as described in the previous section, the impulse components must satisfy the condition whereby $|\xi_x| < \mu|\xi_y|$, so that the tip of the swing leg does not slip relative to the ground at foot contact, which is also discussed in Section 2.5.

The assumptions of this foot contact model are summarized as follows:

FA1. the swing leg has no slip and no rebound at touchdown on the ground.
FA2. the double-supported phase duration ε is infinitesimally short with respect to step cycle τ and time constant δ of the feedback control of the joint motors ($\varepsilon \ll \tau, \delta$).

FA3. the stance foot leaves the ground without interaction.

2.4 Internal oscillator that generates desired joint motions

As described in the introduction, CPG models are widely used to control walking robots. In general, these models use one oscillator for each limb to generate motor commands to activate the limb, which means that the relationship between the oscillator phases represents interlimb coordination [14,50,63]. For example, in quadruped robots, the phase difference between the oscillators explains such gait patterns as walk, pace, trot, and gallop. When biped robots turn to change walking direction during walking, the phase difference between the leg motions plays an important role in achieving adaptive behavior [3]. However, when biped robots walk in a straight line, the leg motions must be out of phase in order to maintain alternating leg behavior. Since the present paper focuses on normal planar walking, we use one oscillator to keep the leg motions out of phase. Let the amplitude and the phase of the oscillator be γ and ϕ, respectively. Referring to [44], we use the following dynamics, which determines the oscillator behavior

$$\dot{\gamma} = -\kappa\omega\gamma(\gamma^2 - s^2)$$
$$\dot{\phi} = \omega \qquad (7)$$

where κ is a gain parameter, ω is a constant frequency, and s is an input parameter. This oscillator dynamics implies that the oscillator has a stable limit cycle, where the oscillator amplitude has asymptotically stable value ($\gamma = s$) and the phase has constant frequency ω.

Physiological findings imply that CPGs consist of hierarchical networks: Rhythm Generator (RG) and Pattern Formation (PF) networks [11,48]. The RG network generates the basic rhythm and alters this rhythm by producing phase shift and rhythm resetting affected by sensory afferents and perturbations. The PF network shapes the rhythm into spatiotemporal patterns of motoneuron activation. Based on these findings, we generate desired joint motions using the rhythmic behavior of the oscillator. More specifically, since human walking behavior must represent such optimality as energy efficiency to generate bipedal walking, we use human-like walking motion for the desired joint motions. In human walking during the swing phase, hip motion generates the basic walking frequency, and the knee motion of the swing leg has a frequency that is approximately double that of the hips [58], which enables clearance to prevent the swing leg from scraping the ground. These motions appear as simple oscillation. Before the swing
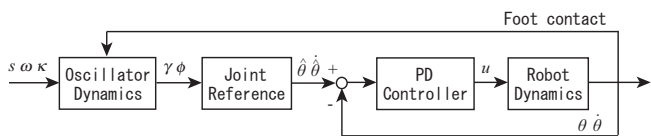
Fig. 2 Block diagram of the control system

Table 1 Physical parameters of the biped robot model

Parameter	Value	Parameter	Value	Parameter	Value
l_a [m]	0.4	m_1 [kg]	3.0	j_1 [kgm^2]	0.2
l_c [m]	0.3	m_2 [kg]	6.0	j_2 [kgm^2]	0.4
		m_3 [kg]	20.0	j_3 [kgm^2]	1.4

leg touches the ground, it stretches the knee joint to prepare for foot contact. Although the knee motion of the stance leg has a double-knee action, its amplitude is too small. Therefore, based on these kinematic characteristics, we use the following desired joint motions:

$$\hat{\theta}_2 = 0$$
$$\hat{\theta}_3 = \gamma \cos \phi$$
$$\hat{\theta}_4 = \gamma \cos \phi$$
$$\hat{\theta}_5 = \begin{cases} \beta\gamma\{1 - \cos\alpha(\phi - \phi_0)\} & 0 \le \alpha(\phi - \phi_0) < 2\pi \\ 0 & \alpha(\phi - \phi_0) \ge 2\pi \end{cases} \quad (8)$$

where the amplitude and phase of the oscillator determine the amplitude and phase of the leg motion, respectively, ϕ_0 is the oscillator phase value just after foot contact, and β determines the amplitude of the knee motions. We use $\alpha \ge 2$ to stretch the knee joint before foot contact. When we use $\beta = 0$, the robot model has no knee motion and the walking behavior becomes similar to that of a compass model. Note that since parameter ω in (7) implies the oscillator frequency, this parameter determines the walking period.

Although joint angles exhibit no sudden changes between just before and just after foot contact, we switch the leg roles between swing and stance at foot contact, as in (4). Therefore, we also need to switch the desired joint angles of the swing and stance legs. Desired state (8) and relationship (4) generate the following conditions for the oscillator states:

$$\gamma^+ = \gamma^-$$
$$\phi^+ = \phi^- - \pi \quad (9)$$

The control scheme by the internal oscillator is shown in Fig. 2.

2.5 Simulation results

In this section, we demonstrate the walking behavior of the biped robot model driven by the oscillator. We use the physical parameters shown in Table 1 and feedback gains κ_i and σ_i ($i = 2, \ldots, 5$) in (2) as follows:

$$\kappa_i = j_2\omega_0^2, \quad \sigma_i = j_2 2\zeta_0\omega_0 \quad i = 2, 5$$
$$\kappa_i = j_3\omega_0^2, \quad \sigma_i = j_3 2\zeta_0\omega_0 \quad i = 3, 4 \quad (10)$$
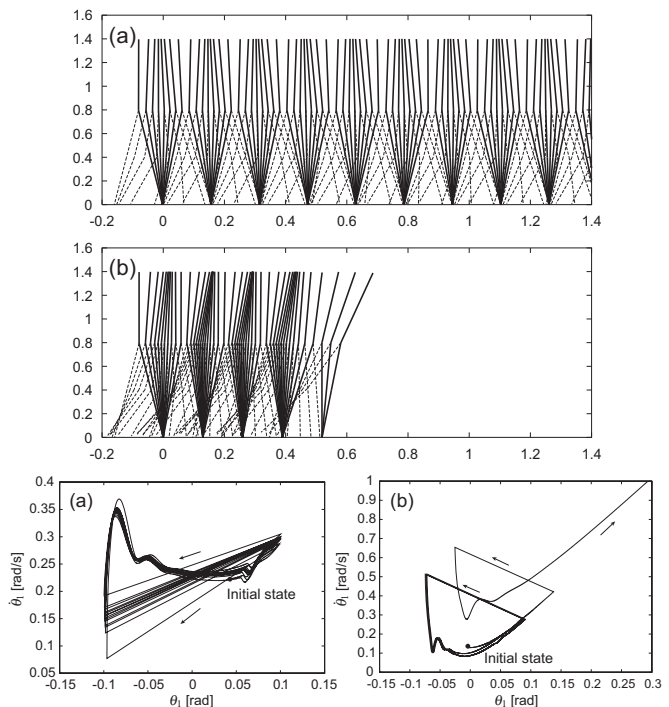

Fig. 3 Stick diagram of walking behavior and postural motion θ_1 and $\dot{\theta}_1$. (a) $\omega = 4.0$ rad. Walking motion converges to periodic motion. (b) $\omega = 2.5$ rad. The walking model falls forward, and the trajectory diverges from periodic behavior.

where we set $\zeta_0 = 0.8$ and $\omega_0 = 40\pi$. The other parameters are as follows: $\kappa = 70$, $\alpha = 2.5$, $\beta = 1.0$, and $s = 0.1$ rad.

In particular, we illustrate two cases of walking speed using frequency ω. Figure 3 shows stick diagrams of the walking behaviors, where the dotted lines indicate the swing leg, and postural motion θ_1 and $\dot{\theta}_1$. In Fig. 3(a), $\omega = 4.0$ rad, where the walking motion converges to a periodic motion, i.e., the walking motion is stable. In Fig. 3(b), $\omega = 2.5$ rad, the model falls forward, and the trajectory in the θ_1-$\dot{\theta}_1$ plane deviates from periodic behavior and diverges, i.e., the walking motion is unstable.

Since we use PD feedback control for the joint movements, the gain parameters influence the walking behavior. In order to investigate the effects of the gain parameters, we calculated the maximum value among
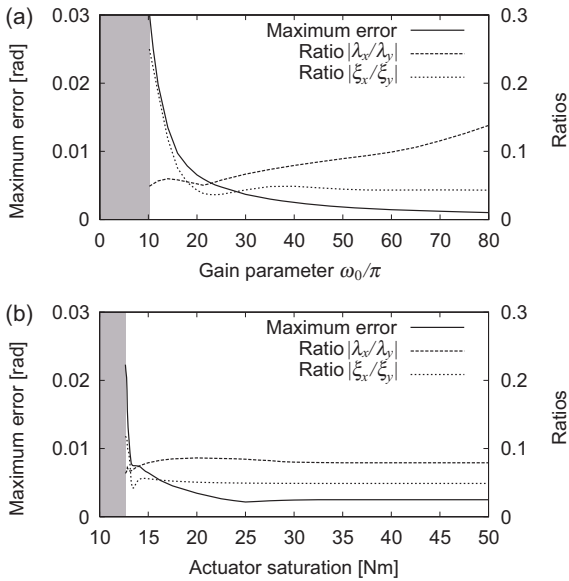
Fig. 4 Effects of gain parameters in (a) joint feedback control and (b) actuator saturation, showing the maximum error among joint errors $|\theta_i - \hat{\theta}_i|$ $(i = 2, \ldots, 5)$ and ratios between horizontal and vertical reaction forces $|\lambda_x/\lambda_y|$ and between horizontal and vertical impulse at foot contact $|\xi_x/\xi_y|$. In the gray area, the walking model falls down.

joint errors $|\theta_i - \hat{\theta}_i|$ $(i = 2, \ldots, 5)$ and the ratios between the horizontal and vertical reaction forces $|\lambda_x/\lambda_y|$ and between the horizontal and vertical impulse at foot contact $|\xi_x/\xi_y|$ for gain parameter ω_0 during stable walking with $\omega = 4.0$ rad in Fig. 4(a). When the parameters are too small, the errors between the joint angles and the desired angles increase, and stable walking cannot be obtained in the light gray area. In contrast, when the parameters are too large, maximum motor torque increases and influences the ground reaction force. However, for a large range of the gain parameters, the joint errors and these ratios remain small. When the static friction coefficient of the ground is larger than these ratios, the stance tip remains constrained on the ground, and the model can establish walking.

In addition to the feedback gains, actuator saturation also influences the walking behavior. In order to examine the effect of actuator saturation, we calculated the maximum value among joint errors and the ratios ($|\lambda_x/\lambda_y|$, $|\xi_x/\xi_y|$) for various actuator saturations in Fig. 4(b). When the saturation is small, the errors between the joint angles and the desired angles increase, and stable walking cannot be obtained in the light gray area. However, when the saturation is not so small, the influence is sufficiently small.

3 Stability characteristics

The numerical simulations in the previous section demonstrated that the proposed biped robot model achieves stable or unstable walking depending on parameters such as walking speed. This section clarifies the stability characteristics of the proposed biped robot by analytically investigating walking behavior. We first conduct an approximate analysis to establish the broad characteristics and then verify these characteristics through rigorous numerical simulations.

3.1 Assumptions for approximate analysis

For approximate analysis, we assume the following:

AA1. the motor controller uses high-gain feedback gains, so that time constant δ of the feedback control is infinitesimally short with respect to step cycle τ $(= \pi/\omega)$ $(\delta \ll \tau)$.

AA2. angles θ_i $(i = 1, \ldots, 5)$ are relatively small during walking.

Assumption AA1 suggests that we can analyze walking behavior when joint angles θ_i and angular velocities $\dot{\theta}_i$ $(i = 2, \ldots, 5)$ are equivalent to the desired states ($\theta_i = \hat{\theta}_i(\gamma, \phi)$, $\dot{\theta}_i = \dot{\hat{\theta}}_i(\gamma, \phi)$). Under this assumption, we can redefine the state variable as $q^{\mathrm{T}} = [\theta_1 \, \dot{\theta}_1 \, \gamma \, \phi]$. That is, the walking behavior is determined by the postural motion (absolute orientation of the robot) and oscillator states. Assumption AA2 implies that we can deal with the equations linearized with respect to the angles.

These assumptions facilitate the analysis of walking motion. However, note that, although assumption AA1 demands that joint angles and angular velocities be equivalent to the desired states, assumptions FA1 through FA3 mentioned in Section 2.3 imply that joint angular velocities suddenly change based on (5) just after foot contact, causing a discrepancy between joint angular velocities by (5) and desired joint angular velocities by (8) and (9), i.e., $\dot{\theta}_i^+ \neq \dot{\hat{\theta}}_i(\gamma^+, \omega^+)$ $(i = 2, \ldots, 5)$. Assumptions FA2 and AA1 suggest that double-supported phase duration ε, time constant δ of the feedback control of the motors, and step cycle τ are related as $\varepsilon \ll \delta \ll \tau$, which means that 1) when the swing leg touches the ground, joint angular velocities change into $\dot{\theta}_i^+$ following (5) in period ε due to foot contact, 2) after which, joint angular velocities change to desired velocities $\dot{\hat{\theta}}_i(\gamma^+, \omega^+)$ following (8) and (9) in period δ due to the feedback control in the motors. That is, joint angular velocities change to desired velocities in period δ $(+\varepsilon) \ll \tau$ from $\dot{\hat{\theta}}_i(\gamma^-, \omega^-)$ to $\dot{\hat{\theta}}_i(\gamma^+, \omega^+)$ $(i =$

2, ..., 5) after foot contact. Although the feedback control torques affect angular velocity $\dot{\theta}_1$ of the posture angle, they are internal forces. Since the model only receives external forces at the swing foot contact point, the angular momentum around this point is conserved during the duration in which joint angular velocities change to desired velocities. Therefore, we can calculate the angular velocity of the posture just after foot contact $\dot{\theta}_1^+$ from angular momentum conservation under the conditions that the joint angles and angular velocities achieve the desired state just before and just after foot contact. The angular momentums around the tips of the legs are derived in Appendix B.

3.2 Approximate equations and solutions

Based on assumptions AA1 and AA2 in the previous section, we reconstruct the equations to achieve approximate periodic solutions. During the swing phase, the joint angles are equivalent to desired states $\theta_i = \hat{\theta}_i(\gamma, \phi)$ $(i = 2, \ldots, 5)$ in (8), and thus linearization of the first row of (1) and (7) gives

$$
\dot{q} = f(q)
$$
$$
= \begin{bmatrix} \dot{\theta}_1 \\ \left\{ \beta_1 \theta_1 - \sum_{i=2}^{5} \left[\alpha_i \ddot{\hat{\theta}}_i(\gamma, \phi) - \beta_i \hat{\theta}_i(\gamma, \phi) \right] \right\}/\alpha_1 \\ -\kappa \omega \gamma (\gamma^2 - s^2) \\ \omega \end{bmatrix} \quad (11)
$$

where

$$
\alpha_i = \sum_{j=i}^{5} a_j, \ \beta_i = \sum_{j=i}^{5} b_j \quad i = 1, \ldots, 5
$$
$$
a_1 = (3m_1/4 + 3m_2 + 2m_3)l_a^2 + m_3 l_a l_c + j_1
$$
$$
a_2 = (m_1/2 + 9m_2/4 + 2m_3)l_a^2 + m_3 l_a l_c + j_2
$$
$$
a_3 = m_3(2l_a + l_c)l_c + j_3
$$
$$
a_4 = -(2m_1 + 3m_2)l_a^2/4 + j_2
$$
$$
a_5 = -m_1 l_a^2/4 + j_1
$$
$$
b_1 = (3m_1/2 + 2m_2 + m_3)l_a g
$$
$$
b_2 = (m_1 + 3m_2/2 + m_3)l_a g
$$
$$
b_3 = m_3 l_c g
$$
$$
b_4 = -(m_1 + m_2/2)l_a g
$$
$$
b_5 = -m_1 l_a g/2
$$

The geometric condition (3) for the swing leg to touch the ground then becomes

$$
r(q) = -\theta_1^2 - \left\{ \theta_1 + \hat{\theta}_2(\gamma, \phi) \right\}^2 + \left\{ \theta_1 + \sum_{i=2}^{4} \hat{\theta}_i(\gamma, \phi) \right\}^2
$$
$$
+ \left\{ \theta_1 + \sum_{i=2}^{5} \hat{\theta}_i(\gamma, \phi) \right\}^2 = 0 \quad (12)
$$

By considering that $\hat{\theta}_2(\gamma, \phi) = \hat{\theta}_5(\gamma, \phi) = 0$ at the foot contact and $\hat{\theta}_3(\gamma, \phi) = \hat{\theta}_4(\gamma, \phi)$ during walking, (12) yields

$$
r(q) = 8\hat{\theta}_3(\gamma, \phi)\left\{ \theta_1 + \hat{\theta}_3(\gamma, \phi) \right\} = 0 \quad (13)
$$

Since $\hat{\theta}_3(\gamma, \phi) = 0$ indicates that the torso and femurs are aligned, we ignore this equation and use

$$
r(q) = \theta_1 + \hat{\theta}_3(\gamma, \phi) = 0 \quad (14)
$$

From the angular momentum conservation, the relationship for angular velocities just before and just after foot contact is given by

$$
\dot{\theta}_1^+ = \dot{\theta}_1^- - \frac{1}{\alpha_1} \sum_{i=2}^{5} \alpha_i \left\{ \dot{\hat{\theta}}_i(\gamma^+, \phi^+) - \dot{\hat{\theta}}_i(\gamma^-, \phi^-) \right\} \quad (15)
$$

Therefore, we obtain the relationship of the states just before and just after foot contact from the first row of (4), (15), and (9) as follows:

$$
q^+ = h(q^-)
$$
$$
= \begin{bmatrix} \theta_1^- + \sum_{i=2}^{5} \hat{\theta}_i(\gamma^-, \phi^-) \\ \dot{\theta}_1^- - \frac{1}{\alpha_1} \sum_{i=2}^{5} \alpha_i \left\{ \dot{\hat{\theta}}_i(\gamma^-, \phi^- - \pi) - \dot{\hat{\theta}}_i(\gamma^-, \phi^-) \right\} \\ \gamma^- \\ \phi^- - \pi \end{bmatrix}
$$
$$
(16)
$$

Based on these equations, the approximate periodic solutions become

$$
\theta_1(t) = \begin{cases} -(k_2 + k_3)\{\cosh(\lambda\Delta)\sinh(\lambda t)/\sinh(\lambda\tau) \\ \quad -\sinh(\lambda(t-\tau))/\sinh(\lambda\tau)\} \\ \quad +(s + k_1)\cos\phi_0 \sinh(\lambda(t-\frac{\tau}{2}))/\sinh(\lambda\frac{\tau}{2}) \\ \quad +k_1\cos\phi(t) + k_2\cos\alpha\{\phi(t) - \phi_0\} + k_3 \\ \qquad\qquad\qquad\qquad\quad \text{for } 0 \leq t \leq t_0 \\ -(k_2 + k_3)\{\cosh(\lambda\Delta)\sinh(\lambda t)/\sinh(\lambda\tau) \\ \quad -\sinh(\lambda(t-\tau))/\sinh(\lambda\tau) - \cosh(\lambda(t-t_0))\} \\ \quad +(s + k_1)\cos\phi_0 \sinh(\lambda(t-\frac{\tau}{2}))/\sinh(\lambda\frac{\tau}{2}) \\ \quad +k_1\cos\phi(t) \qquad\qquad\quad \text{for } t_0 \leq t \leq \tau \end{cases}
$$
$$
\gamma(t) = s \quad \text{for } 0 \leq t \leq \tau
$$
$$
\phi(t) = \omega\tau + \phi_0 \quad \text{for } 0 \leq t \leq \tau \quad (17)
$$

where $t = 0$ is the time just after foot contact, $t = t_0 (= \frac{2\pi}{\alpha\omega} \leq \tau)$ is the time when the swing leg stretches the knee joint, $t = \tau(= \pi/\omega)$ is the time just before the next foot contact, and

$$
\lambda = \sqrt{\beta_1/\alpha_1}
$$
$$
\Delta = \tau - t_0
$$
$$
k_1 = -\frac{\beta_3 + \beta_4 + (\alpha_3 + \alpha_4)\omega^2}{\beta_1 + \alpha_1\omega^2} s
$$
$$
k_2 = \frac{\beta_5 + \alpha^2 \alpha_5 \omega^2}{\beta_1 + \alpha^2 \alpha_1 \omega^2} \beta s
$$
$$
k_3 = -\frac{\beta_5}{\beta_1} \beta s
$$
$$
\phi_0 = \sin^{-1} \frac{\lambda(k_2 + k_3)\sinh(\lambda t_0/2)\cosh(\lambda\Delta/2)}{\{k_1 + s(\alpha_3 + \alpha_4)/\alpha_1\}\omega\cosh(\lambda\tau/2)}
$$

Note that solution $\theta_1(t)$ satisfies the continuities of the angle and angular velocity at $t = t_0$. Using these solutions, approximate periodic solutions for the horizontal λ_x and vertical λ_y ground reaction forces are given as

$$\lambda_x = \{m_3 l_c + (m_1 + 3m_2 + 2m_3)l_a\}\ddot{\theta}_1$$
$$+ \{m_3 l_c - (3m_1 + m_2)l_a/2\}\ddot{\theta}_3$$
$$- (3m_1 + m_2)l_a\ddot{\theta}_4/2 - m_1 l_a\ddot{\theta}_5/2$$
$$\lambda_y = \{2(m_1 + m_2) + m_3\}g \qquad (18)$$

Figure 5 compares the approximate periodic solutions and rigorous simulation results using the original equations without incorporating assumptions AA1 and AA2, where we used $\omega = 4.0$ rad and the same values for the other parameters, as in Section 2.5. Figures 5(a) and (b) show angles $\theta_1 \cdots \theta_5$ and oscillator states γ and ϕ, where the approximate solutions establish results similar to those obtained through the numerical simulations, verifying the validity of the approximate analysis. Figure 5(c) shows the horizontal and vertical reaction forces from the ground. Since the approximate analysis is based on a linear analysis of angles, the approximate solution for the vertical reaction force becomes constant and induces a discrepancy between the approximate solution and the rigorous simulation result. The horizontal reaction force differs for the approximate solution and the simulation result from 0 to 0.2 s, as a result of the feedback control torque due to the discrepancy between the joint angular velocities and the desired states just after foot contact, as mentioned in Section 3.1. Figure 5(d) shows the ratio between the horizontal and vertical reaction forces, where the maximum magnitude is 0.079. The simulation result for the impulse at foot contact is $|\xi_x/\xi_y| = 0.047$. Therefore, when the static friction coefficient of the ground is larger than 0.079, the tip of the stance leg remains constrained on the ground, and the model can establish walking behavior.

3.3 Stability analysis using Poincaré map

In this section, we investigate the stability characteristics of walking behavior. In particular, we examine local stability using the obtained approximate periodic solutions and a Poincaré map, where we use the state just after foot contact as the state on the Poincaré section. A Poincaré map is the return map from one point on the Poincaré section to the next point on the Poincaré section. Periodic behavior results in a fixed point on the Poincaré section, and stability is determined from the eigenvalues of the Jacobian matrix of the Poincaré map around the fixed point. Periodic motion is asymptotically stable if all of the eigenvalues are inside the unit
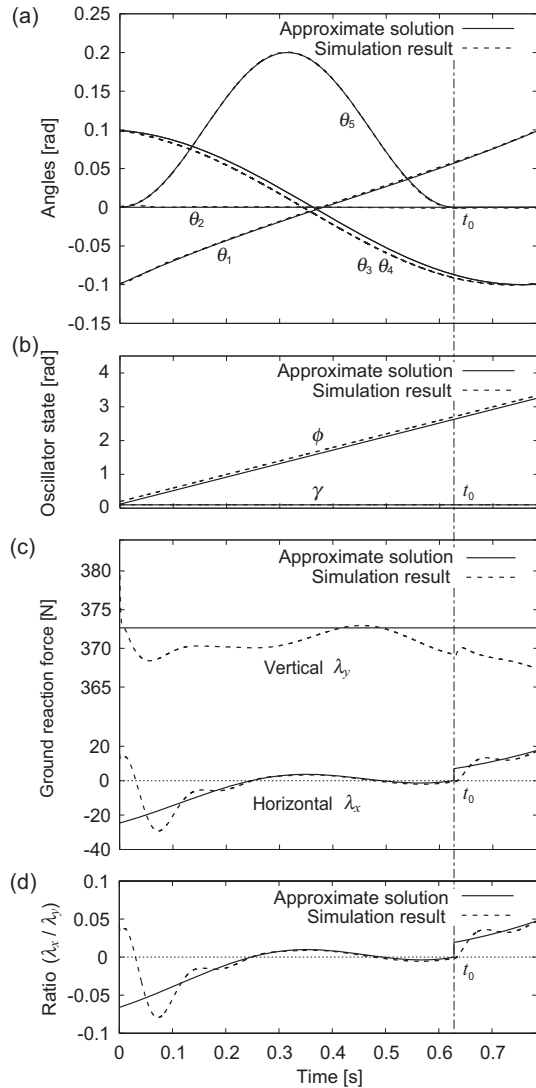
Fig. 5 Comparison between approximate solutions and simulation results. (a) Angles, (b) oscillator states, and (c) ground reaction forces. (d) Ratio between horizontal and vertical reaction forces.

circle on the complex plane, i.e., all of the magnitudes of the eigenvalues are less than 1.

Here, we derive the Jacobian matrix of the Poincaré map using the obtained periodic solutions. Since walking motion is governed by continuous and discrete equations, the Jacobian matrix is affected by such a hybrid structure. By following the derivation given by Coleman et al. [13], Jacobian matrix $\mathcal{J}$ can be calculated as the product of the three matrices induced by the disturbances in the discrete changes due to the foot contact, the change in its timing, and the evolved perturbations during the continuous equation. From the obtained periodic solutions, Jacobian matrix $\mathcal{J}$ is given by (see

Appendix C)

$$\mathcal{J} = \begin{bmatrix} J_{11} & J_{12} & \star & J_{14} \\ J_{21} & J_{22} & \star & J_{24} \\ 0 & 0 & e^{-2\kappa\omega s^2\tau} & 0 \\ J_{41} & J_{42} & \star & J_{44} \end{bmatrix} \tag{19}$$

where $\star$ does not influence the calculation of eigenvalues,

$J_{1i} = J_{4i}s\sin\phi_0 \quad i = 1, 2, 4$

$J_{21} = -\{\ddot{\theta}_1^*(\tau) + B_{24}\omega\}\cosh(\lambda\tau)/D_0 + \lambda\sinh(\lambda\tau)$

$J_{22} = -\{\ddot{\theta}_1^*(\tau) + B_{24}\omega\}\sinh(\lambda\tau)/(\lambda D_0) + \cosh(\lambda\tau)$

$J_{24} = -\{\cosh(\lambda\tau) + 1\}\{[\ddot{\theta}_1^*(\tau) + B_{24}\omega]\epsilon_6\sin\phi_0/D_0$
$\qquad -\epsilon_6\omega\cos\phi_0 - \epsilon_7\} - \sinh(\lambda\tau)\{[\ddot{\theta}_1^*(\tau) + B_{24}\omega]$
$\qquad \times(\epsilon_6\omega\cos\phi_0 + \epsilon_7)/(\lambda D_0) - \epsilon_6\lambda\sin\phi_0\}$
$\qquad -\{\cosh(\lambda\Delta) + 1\}\epsilon_7 + \sinh(\lambda\Delta)\{\ddot{\theta}_1^*(\tau) + B_{24}\omega\}$
$\qquad \times\epsilon_7/(\lambda D_0) - \{\ddot{\theta}_1^*(\tau)s\sin\phi_0 - B_{24}\dot{\theta}_1^*(\tau)\}/D_0$

$J_{41} = -\omega\cosh(\lambda\tau)/D_0, \quad J_{42} = -\omega\sinh(\lambda\tau)/(\lambda D_0)$

$J_{44} = -\omega\{\epsilon_6[(\cosh(\lambda\tau) + 1)\sin\phi_0 + \sinh(\lambda\tau)\omega\cos\phi_0/\lambda]$
$\qquad +\epsilon_7[\sinh(\lambda\tau) - \sinh(\lambda\Delta)]/\lambda\}/D_0 + \dot{\theta}_1^*(\tau)/D_0$

and $(\ )^*$ is the periodic solution obtained using (17). Note that we calculate Jacobian matrix $\mathcal{J}$ by incorporating all perturbations for the state variables without confining them to the Poincaré section.

Matrix $\mathcal{J}$ has four eigenvalues $\Lambda_1 \cdots \Lambda_4$. One of these eigenvalues is $\Lambda_1 = 0$, which reflects the eigenvalue for which the eigenvector is perpendicular to the Poincaré section. In other words, $\delta\theta_1 + \cos\phi^*(0)\delta\gamma - \gamma^*(0)\sin\phi^*(0)\delta\phi = 0$, where δz is the perturbation of state z. The second of these eigenvalues is $\Lambda_2 = e^{-2\kappa\omega s^2\tau}$ (< 1). The other eigenvalues, $\Lambda_{3,4}$, are calculated as follows:

$$\Lambda^2 - (J_{22} + J_{44} + s\sin\phi_0 J_{41})\Lambda + J_{22}J_{44} - J_{24}J_{42}$$
$$-s\sin\phi_0(J_{21}J_{42} - J_{22}J_{41}) = 0 \tag{20}$$

These calculated eigenvalues indicate that when $\max_{i=3,4}|\Lambda_i| < 1$, periodic walking is asymptotically stable; otherwise it is unstable.

The calculated eigenvalues explain the stability of the walking behavior. In the following, we investigate the effects of the knee motion, the torso, and the locomotion speed on walking stability.

3.3.1 Effects of knee motion

As described in Section 2.4, the knee motion during the swing phase produces clearance to prevent the swing leg from scraping the ground. In addition to this geometric role, we examine the dynamic effects of the knee motion on walking stability with parameter β to change the knee amplitude. For the other parameters, we use the values described in Section 2.5.

Figure 6(a) shows the maximum eigenvalue between Λ_3 and Λ_4 for knee amplitude β and locomotor frequency ω, where the light gray area is the unstable region ($\max_{i=3,4}|\Lambda_i| > 1$) and the dark gray area is calculated by numerical simulations, in which the swing leg scrapes the ground because the knee motion is small. Note that, in the dark gray area, we calculate the eigenvalues by ignoring the foot scrapes and that, since $\Lambda_2 = e^{-2\kappa\omega s^2\tau}$ is 0.012, the maximum eigenvalue of Jacobian matrix $\mathcal{J}$ is determined from Λ_3 and Λ_4. The bold and dotted lines are the stability boundaries of the approximate analysis and the rigorous simulation results, respectively, which establish similar results and verify the validity of the stability analysis. This figure indicates that the increased locomotion speed decreases the maximum eigenvalue and that a threshold exists for the locomotion speed to stabilize walking behavior. In addition, the increased knee amplitude decreases the maximum eigenvalue, although it is approximately constant in the stability region. That is, the increased locomotion speed and knee amplitude increase walking stability. When we use $\beta = 0$, there is no knee motion and the walking behavior resembles a compass model. The maximum eigenvalue is larger than or equal to 1, and the model cannot achieve sufficient stability, as obtained in [4].

This analysis reveals that knee motion contributes to the generation of walking behavior not only by producing clearance to prevent the swing leg from scraping the ground but also by increasing stability due to its dynamic effects.

3.3.2 Effects of the torso

Next, we investigate the effects of the torso. We retained total mass $2(m_1 + m_2) + m_3$ and changed the mass ratio $m_3/\{2(m_1 + m_2)\}$. Thus, when this mass ratio increases, the mass ratio of the torso increases. For the moments of inertia, we used $j_1 = 0.2m_1/3.0$ kgm², $j_2 = 0.4m_2/6.0$ kgm², and $j_3 = 1.4m_3/20$ kgm².

Figure 6(b) shows the maximum eigenvalue between Λ_3 and Λ_4 for the mass ratio and locomotor frequency ω, where the light gray area is the unstable region ($\max_{i=3,4}|\Lambda_i| > 1$). The bold and dotted lines are the stability boundaries of the approximate analysis and the rigorous simulation results, respectively, which also establish similar results and verify the validity of the stability analysis. This figure reveals that increased locomotion speed decreases the maximum eigenvalue and that a threshold exists for the locomotion speed. Although the increased mass ratio of the torso increases the stable region, it also increases the maximum eigenvalue in the stable region.
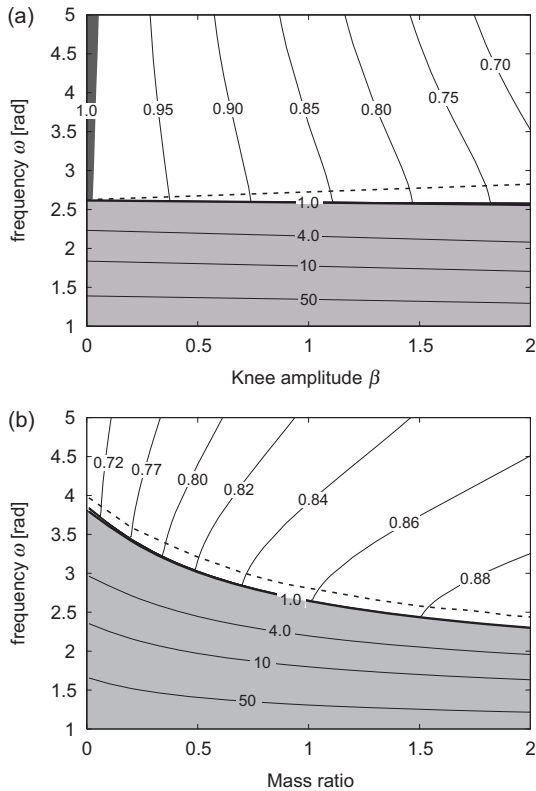
Fig. 6 Maximum eigenvalue between Λ_3 and Λ_4. The light gray area is the unstable region, and, in the dark gray area, the swing leg scrapes during walking. The bold and dotted lines indicate the stability boundaries of the approximate analysis and rigorous simulation results, respectively. (a) Effects of knee motion and locomotion speed. (b) Effects of the mass ratio of the torso and the locomotion speed.

4 Stability improvement by phase resetting

In the previous section, we investigated the stability characteristics of walking behavior driven by an internal oscillator, where we generated joint motions using the rhythmic behavior of the oscillator states. Since the oscillator did not modulate its own behavior by sensory information, the walking behavior was open-loop. However, the walking behavior should be generated through the dynamic interactions among the robot, the oscillator, and the environment. Therefore, in this section, we improve the walking behavior by incorporating a phase resetting mechanism using foot-contact information.

4.1 Phase resetting

As mentioned in Section 2.4, the RG network in CPGs creates the basic rhythm, and the PF network produces the patterns of signals from the rhythm information from the RG network to be delivered to the motoneurons. The RG network modulates the basic rhythm by producing phase shift and rhythm resetting affected by sensory afferents and perturbations. Since the PF network produces signal patterns based on the rhythm information from the RG network, such modulation of the basic rhythm affects signal generation in the PF network. Such phase and rhythm modulation plays an important role in generating adaptive walking behavior. Yamasaki *et al.* [61] and Aoi *et al.* [8, 9] simulated human bipedal walking and examined robustness against force disturbances. They prepared joint angles or motor commands encoded by the oscillator phase, and modulated the joint motions or motor commands by resetting the oscillator phase when disturbed. Their simulation illustrates that such phase resetting prevents falling against postural disturbances induced by perturbations and increases stability.

In robotics research, a number of studies have demonstrated the advantage of phase resetting to achieve stable walking using biped robots [2, 3, 6, 40, 41]. In particular, phase reset followed by foot contact is effective, resulting in smooth transition from the swing to stance phases. Therefore, in the following section, we incorporate such a phase resetting mechanism using foot-contact information.

4.2 Phase resetting model

Just after foot contact, we reset the oscillator phase to ϕ_0, obtained by numerical simulations and approximate analysis, as follows:

$$\phi^+ = \phi_0 \qquad (21)$$

Accompanied by this phase resetting, we modulated the oscillator amplitude to avoid inducing discrete changes in the desired joint angles by

$$\gamma^+ = -\gamma^- \cos\phi^- / \cos\phi^+ \qquad (22)$$

Therefore, among the governing equations in Section 2, only (9) changes.

4.3 Stability characteristics

In this section, we examine the stability characteristics of walking behavior by incorporating phase resetting. As in Section 3, we analyze the stability characteristics based on an approximate analysis using the same assumptions and then verify the obtained results through rigorous numerical simulations.

Due to (21) and (22), only (16) in the approximate equations in Section 3.2 changes to

$$q^+ = \tilde{h}(q^-)$$
$$= \begin{bmatrix} \theta_1^- + \sum_{i=2}^5 \hat{\theta}_i(\gamma^-, \phi^-) \\ \dot{\theta}_1^- - \frac{1}{\alpha_1}\sum_{i=2}^5 \alpha_i \left\{ \dot{\hat{\theta}}_i(\gamma^-, \phi^- - \pi) - \dot{\hat{\theta}}_i(\gamma^-, \phi^-) \right\} \\ -\gamma^- \cos\phi^- / \cos\phi_0 \\ \phi_0 \end{bmatrix}$$
(23)

Since this change does not influence the approximate solutions, we achieve the same solutions as (17).

In order to investigate the stability characteristics, we derive the Jacobian matrix in the manner described in Section 3.3. Jacobian matrix $\tilde{\mathcal{J}}$ with phase resetting is given by (see Appendix C)

$$\tilde{\mathcal{J}} = \begin{bmatrix} \tilde{J}_{11} & \tilde{J}_{12} & \tilde{J}_{13} & \star \\ \tilde{J}_{21} & \tilde{J}_{22} & \tilde{J}_{23} & \star \\ \tilde{J}_{31} & \tilde{J}_{32} & \tilde{J}_{33} & \star \\ 0 & 0 & 0 & 0 \end{bmatrix}$$
(24)

where $\star$ does not influence the calculation of the eigenvalues,

$$\tilde{J}_{1i} = J_{1i} \quad i = 1, 2$$
$$\tilde{J}_{13} = (s\omega \sin\phi_0/D_0 - 1)\cos\phi_0 e^{-2\kappa\omega s^2 \tau} - s\omega \sin\phi_0 E_{13}/D_0$$
$$\tilde{J}_{21} = -\{\ddot{\theta}_1^*(\tau) + \tilde{B}_{24}\omega\}\cosh(\lambda\tau)/D_0 + \lambda\sinh(\lambda\tau)$$
$$\tilde{J}_{22} = -\{\ddot{\theta}_1^*(\tau) + \tilde{B}_{24}\omega\}\sinh(\lambda\tau)/(\lambda D_0) + \cosh(\lambda\tau)$$
$$\tilde{J}_{23} = -\{\ddot{\theta}_1^*(\tau) + \tilde{B}_{24}\omega\}E_{13}/D_0 + E_{23}$$
$$\qquad + \{[\ddot{\theta}_1^*(\tau) + \tilde{B}_{24}\omega]\cos\phi_0/D_0 + \tilde{B}_{23}\}e^{-2\kappa\omega s^2 \tau}$$
$$\tilde{J}_{3i} = -\tilde{J}_{1i}/\cos\phi_0 \quad i = 1, 2, 3$$

Matrix $\tilde{\mathcal{J}}$ has four eigenvalues $\tilde{\Lambda}_1 \cdots \tilde{\Lambda}_4$. Two of these eigenvalues are zero, that is, $\tilde{\Lambda}_{1,2} = 0$, and the other two, $\tilde{\Lambda}_{3,4}$, are calculated as follows:

$$\tilde{\Lambda}^2 - (\tilde{J}_{22} + \tilde{J}_{33} - \cos\phi_0\tilde{J}_{31})\tilde{\Lambda} + \tilde{J}_{22}\tilde{J}_{33} - \tilde{J}_{23}\tilde{J}_{32}$$
$$+ \cos\phi_0(\tilde{J}_{21}\tilde{J}_{32} - \tilde{J}_{22}\tilde{J}_{31}) = 0$$
(25)

Therefore, when $\max_{i=3,4}|\tilde{\Lambda}_i| < 1$, periodic walking is asymptotically stable; otherwise it is unstable.

Figures 7(a) and (b) show the maximum eigenvalue between $\tilde{\Lambda}_3$ and $\tilde{\Lambda}_4$ for knee amplitude β and locomotor frequency ω and for the mass ratio of the torso and locomotor frequency ω, respectively, where the light gray area indicates the unstable region ($\max_{i=3,4}|\tilde{\Lambda}_i| > 1$) and the dark gray area is the area calculated by numerical simulations, where the swing leg scrapes the ground, because the knee motion is small. The bold and dotted lines are the stability boundaries of the approximate analysis and rigorous simulation results, respectively, which achieve similar results and verify the validity of this analysis. Compared to Figs. 6(a) and
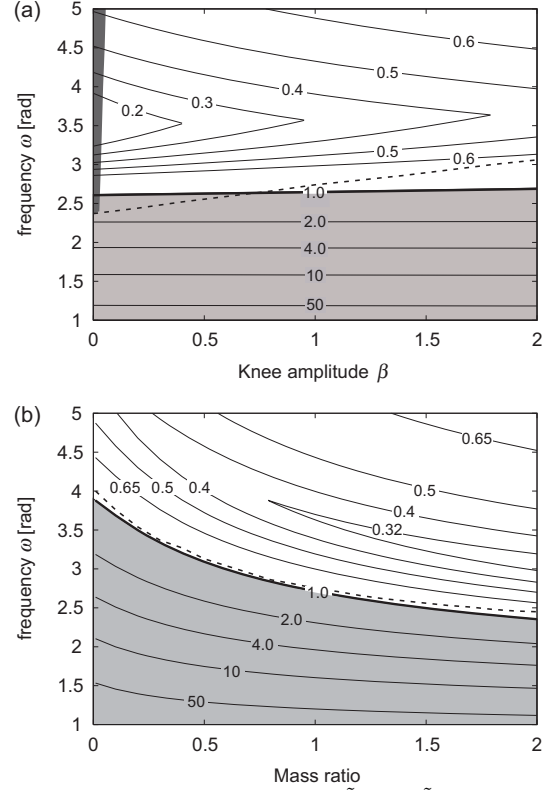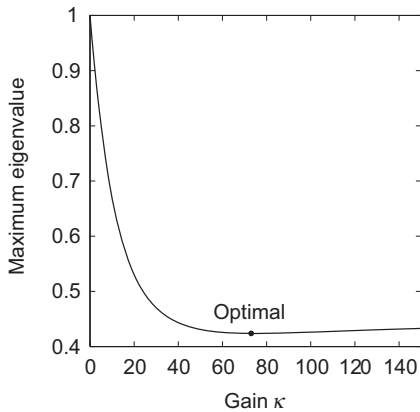

Fig. 7 Maximum eigenvalue between $\tilde{\Lambda}_3$ and $\tilde{\Lambda}_4$. The light gray area indicates the unstable region, and dark gray area indicates the area in which the swing leg scrapes during walking. The bold and dotted lines indicate the stability boundaries of the approximate analysis and the rigorous simulation results, respectively. (a) Knee amplitude and locomotion speed. (b) Mass ration of the torso and locomotion speed.

(b), which do not incorporate phase resetting, the stability structure is greatly changed. Although the stable regions for parameters exhibit almost no change, the maximum eigenvalue decreases, which verifies the stability improvement due to the modulation of oscillator states based on phase resetting using foot-contact information, as in [6].

4.4 Optimization

Walking behavior is generated through the interactions among the robot dynamics, the oscillator dynamics, and the environment. Although such interactions are crucial, there is no guiding principle for designing these interactions. As described above, the proposed model produced the interactions by the modulation of the oscillator phase due to phase resetting using foot-contact information, which played an important role in producing stable walking, as investigated in the previous section. When the oscillator phase is reset, the oscillator

Fig. 8 Optimal value for gain parameter κ to minimize the maximum eigenvalue
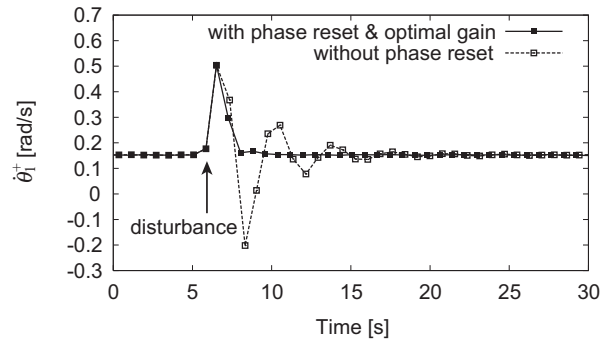

Fig. 9 Behavior of angular velocity $\dot{\theta}_1^+$ of the posture angle just after foot contact, for the case of the addition of a disturbance

amplitude is also modulated as describe in (22). The amplitude follows its dynamics (7) and asymptotically approaches a stable value, s, which modifies the robot motion and results in stability improvement. As shown in (7), gain parameter κ represents the strength of the interactions. Therefore, determining this parameter is important in order to adequately exploit the interactions to generate stable walking.

Figure 8 shows the maximum eigenvalue between $\tilde{\Lambda}_3$ and $\tilde{\Lambda}_4$ for gain parameter κ, where we used $\omega = 4.0$ rad and the other parameters are as shown in Section 2.5. The maximum eigenvalue is minimized at $\kappa = 74$, indicating that we can obtain optimal interactions from the viewpoint of stability. When we used $\kappa = 0$, there is no such interaction and the maximum eigenvalue becomes 1, which reflects that the model cannot achieve sufficient stability. Figure 9 shows the behavior of angular velocity $\dot{\theta}_1^+$ of the posture angle just after foot contact with and without phase resetting using the optimal gain obtained by numerical simulations by adding a disturbance, which demonstrates that the rate of convergence increases using phase resetting and optimal gain.

5 Discussion

5.1 Locomotion control using an oscillator

In the present paper, we investigated the stability characteristics of the walking behavior of a five-link planar biped robot. We used an internal oscillator that has a stable limit cycle and generated joint motions using the oscillator states. Although the robot does not require any actuators or sensors to directly control and monitor postural motion (absolute orientation of the robot), stable walking is achieved depending on param-

eters such as walking speed, knee amplitude, and distribution of mass. Furthermore, we used foot-contact information that intermittently occurs during walking and modulated the oscillator states based on the information using phase resetting, which improved walking stability. Although limit cycle oscillators, such as the van der Pol oscillator, have been used to control biped robots [17, 18, 32, 64], the obtained results show that walking behavior is improved through the interactions among the robot dynamics, the oscillator dynamics, and the environment.

In previous studies, we used an actual biped robot without actuators and sensors to directly control the postural behavior and developed its locomotion controller using oscillators as in the present study [2,3]. We generated desired joint motions using oscillator phases and modulated them based on phase resetting using foot-contact information, which achieved adaptive walking behaviors. As mentioned above, although many researchers created sophisticated biped robots and control systems, most generated robot motions based on criteria such as zero moment point [56], which requires accurate modeling of both the robot and the environment and complicated computations. However, the proposed controller does not need such modeling or calculations and its control scheme is simple. The present paper follows the approach of our previous studies and demonstrates the advantages of a control system using oscillators.

5.2 Contraction of state variables

In the present study, we created desired joint motions by oscillator states and controlled joints using PD feedback control. Since we used high-gain feedback gains, we assumed that the joints achieved the desired states in the approximate analysis, resulting in the descrip-

tion of joint states by the oscillator states. Therefore, we can only describe walking behavior by the postural motion (absolute orientation of the robot) and the oscillator states. Since the oscillator originally has a stable limit cycle, the stability depends on the postural behavior that is driven by periodic motions of the joints, gravitational force, and foot contact events. Depending on the walking speed, knee amplitude, and distribution of mass, the relationship among their dynamic contributions changes, which influences the stability characteristics. Although high-gain feedback control and oscillator-driven walking behavior result in such contraction of the state variables, when we use a much larger value for feedback gains, the maximum feedback torque also becomes large, which affects the ground reaction force, and the ratio between the horizontal and vertical components increases. Therefore, we must carefully treat the feedback gains.

Regarding the stabilization of planar biped robots, Grizzle *et al.* [24] and Westervelt *et al.* [57] used three- and five-link biped models without actuators on the feet to directly control the postural movement (absolute orientation of the robot). However, they did consider robots that could directly monitor the postural behavior. They successfully established stable bipedal walking by incorporating finite-time stabilizing feedback control and zero dynamics and contracting robot states based on the postural state. In the present paper, the robot was not aware of its postural movements, which makes it more difficult to create stable walking, and postural behavior was determined through dynamics affected by the joint motions described by the oscillator states. Therefore, we dealt with the posture and oscillator states separately.

5.3 Relationship with passive dynamic walking

Passive dynamic walking is a common walking model in which a robot walks down a shallow slope using only the energy of gravity [39]. The robot requires no actuators or sensors and has self-stability as an inherent dynamic characteristic [20]. Using such characteristics, a number of studies have established efficient and natural walking behaviors [10, 15, 21, 34]. The walking behavior of passive dynamic walking depends heavily on inertia and gravity forces. Body motion relative to the stance foot appears as an inverted pendulum, and the swing leg resembles a swinging pendulum. The foot contact event changes the roles of the legs and starts at the next step, and stable walking is generated through interaction between the robot mechanical system and the ground. On the other hand, the swing leg of the proposed model is driven primarily by an oscillator that has

inherent frequency, which enables the walking speed to be changed. The oscillator receives foot-contact information and modulates walking behavior. The proposed model establishes stable walking through interaction among the robot mechanical system, the oscillator, and the ground.

5.4 Advanced control scheme

We used only one oscillator, which forced the right and left legs to be out of phase. Although this produced stable walking behavior and the stability was improved due to phase resetting, further investigation of the adaptive functions was not possible due to the coordination between the legs. Since such coordination plays an important role in generating adaptive walking behavior [3], we must investigate and clarify this mechanism in future studies.

In order to investigate the effects of the interactions among the robot, the oscillators, and the environment in the generation of locomotion of biped robots, we did not explicitly incorporate the posture control to maintain the pitch of the torso vertical using such sensors as a gyro sensor and a ground reaction force sensor. Therefore, the stability was limited. However, the obtained stable walking reveals that the designed joint motions create adequate postural motion and that the modulation of the oscillator states using phase resetting contributes to improved stability. In order to further increase the stability, we must incorporate adequate posture control in the future. Furthermore, although we fixed the value for the oscillator phase to be reset, appropriate determination of the reset value, which changes the periodic motion, will improve the stability characteristics [6].

In locomotion control using oscillators, interactions among the robot, the oscillators, and the environment are crucial. The proposed model generated these interactions through phase resetting, and we examined parameter optimization to adequately exploit these interactions. Although designing such interactions is difficult, more advanced and sophisticated interactions will create adaptive functions.

6 Conclusion

In the present paper, we investigated the stability characteristics of the walking behavior of a five-link planar biped robot driven by an internal oscillator. The robot achieved stable walking depending on parameters that revealed the contributions of the knee motion and the

torso to walking stability. We verified the stability improvement due to the modulation of oscillator states based on phase resetting using foot-contact information. Furthermore, we investigated the parameter optimization in order to adequately exploit the interactions among the robot dynamics, the oscillator dynamics, and the environment in achieving adaptive walking. These results illustrate the advantages and usefulness of locomotion control using oscillators.

A Equations for the biped robot model

In this appendix, we show the governing equations for the biped robot model. First, we derive the equation of motion for generalized state variables that includes the position of the tip of the stance leg relative to the ground.

To derive the equation, we introduce the following distance vectors: $r_1 = [\,0\ l_a\,]^T$, $r_2 = [\,0\ l_a\,]^T$, $r_3 = [\,0\ 0\,]$, $r_4 = [\,0\ -l_a\,]^T$, $r_5 = [\,0\ -l_a\,]^T$, $w_i = r_i/2$ $(i = 1, 2, 4, 5)$, and $w_3 = [\,0\ l_c\,]^T$, where r_i is the distance vector between joints and w_i is the distance vector from a joint to a center of mass. Using the Lagrangian equation, the equation of motion for generalized state variable $\bar{q}^T = [\,x\ y\ \theta_1\ \theta_2\ \theta_3\ \theta_4\ \theta_5\,] \in \mathbb{R}^7$ is derived as

$$\bar{K}(\bar{q})\ddot{\bar{q}} + \bar{c}(\bar{q}, \dot{\bar{q}}) + \bar{\nu}(\bar{q}) = \bar{u}(\bar{q}, \dot{\bar{q}}) + \bar{\lambda} \tag{26}$$

where x and y are the horizontal and vertical positions of the tip of the stance leg, respectively, $\bar{K}(\bar{q}) \in \mathbb{R}^{7 \times 7}$ is the inertia matrix, $\bar{c}(\bar{q}, \dot{\bar{q}}) \in \mathbb{R}^7$ is the nonlinear term, $\bar{\nu}(\bar{q}) \in \mathbb{R}^7$ is the gravity term, $\bar{u}(\bar{q}, \dot{\bar{q}}) \in \mathbb{R}^7$ is the input torque term, and $\bar{\lambda} \in \mathbb{R}^7$ is the ground reaction force term (impulsive force term at foot contact). Inertia matrix $\bar{K}(\bar{q})$ is given as

$$\bar{K}(\bar{q}) = H^T\{L(\bar{q})^T M L(\bar{q}) + J\}H \tag{27}$$

where

$$H = \begin{bmatrix} I_{2\times2} & \\ & 1 \\ & \vdots & \ddots \\ & 1 \cdots 1 \end{bmatrix} \in \mathbb{R}^{7 \times 7}$$

$$L(\bar{q}) = L_1(\bar{q}) + L_2 \in \mathbb{R}^{10 \times 7}$$

$$L_1(\bar{q}) = \begin{bmatrix} R_{1,0}(\bar{q}) & o & & \\ R_{2,0}(\bar{q}) & R_{2,1}(\bar{q})\tilde{r}_1 & o & \\ \vdots & \vdots & \ddots & \ddots \\ R_{5,0}(\bar{q}) & R_{5,1}(\bar{q})\tilde{r}_1 & \cdots & R_{5,4}(\bar{q})\tilde{r}_4 & o \end{bmatrix}$$

$$L_2 = \begin{bmatrix} & \tilde{w}_1 & & \\ O_{10\times2} & & \ddots & \\ & & & \tilde{w}_5 \end{bmatrix}$$

$$M = \mathrm{diag}[\,m_1\ m_1\ m_2\ m_2\ m_3\ m_3\ m_2\ m_2\ m_1\ m_1\,] \in \mathbb{R}^{10 \times 10}$$

$$J = \mathrm{diag}[\,0\ 0\ j_1\ j_2\ j_3\ j_2\ j_1\,] \in \mathbb{R}^{7 \times 7}$$

Here, $I_{n\times n} \in \mathbb{R}^{n \times n}$ is a unit matrix, $O_{m\times n} \in \mathbb{R}^{m \times n}$ and $o \in \mathbb{R}^{2 \times 1}$ are zero matrices, and $R_{i,j}(\bar{q}) \in \mathbb{R}^{2 \times 2}$ $(i, j = 0, \ldots, 5, i > j)$ is a rotation matrix given as

$$R_{i,j}(\bar{q}) = \begin{bmatrix} \cos\theta_{i,j}(\bar{q}) & \sin\theta_{i,j}(\bar{q}) \\ -\sin\theta_{i,j}(\bar{q}) & \cos\theta_{i,j}(\bar{q}) \end{bmatrix} \quad i, j = 0, \ldots, 5,\ i > j$$

where

$$\theta_{i,j}(\bar{q}) = \sum_{k=j+1}^{i} \theta_k$$

and for $z = [\,z_1\ z_2\,]^T$, $\tilde{z}$ is expressed as $\tilde{z} = [\,-z_2\ z_1\,]^T$. Note that $\bar{K}(\bar{q})\dot{\bar{q}}$ is a vector denoting the generalized momentum of this system. Nonlinear term $\bar{c}(\bar{q}, \dot{\bar{q}})$ becomes

$$\bar{c}(\bar{q}, \dot{\bar{q}}) = \bar{K}_t(\bar{q}, \dot{\bar{q}})\dot{\bar{q}} + V(\bar{q}, \dot{\bar{q}})p(\bar{q}, \dot{\bar{q}}) \tag{28}$$

where

$$\bar{K}_t(\bar{q}, \dot{\bar{q}}) = \dot{\bar{K}}(\bar{q})$$

$$V(\bar{q}, \dot{\bar{q}}) = \begin{bmatrix} O_{2\times10} \\ \tilde{v}_1^T(\bar{q}, \dot{\bar{q}}) \\ & \ddots \\ & & \tilde{v}_5^T(\bar{q}, \dot{\bar{q}}) \end{bmatrix} \in \mathbb{R}^{7 \times 10}$$

$$[\,v_1^T(\bar{q}, \dot{\bar{q}}) \ldots v_5^T(\bar{q}, \dot{\bar{q}})\,]^T = L_1(\bar{q})H\dot{\bar{q}} \in \mathbb{R}^{10}$$

$$p(\bar{q}, \dot{\bar{q}}) = B(\bar{q})^T M L(\bar{q})H\dot{\bar{q}} \in \mathbb{R}^{10}$$

$$B(\bar{q}) = \begin{bmatrix} I & & & \\ R_{2,1}(\bar{q}) & I & & \\ \vdots & \ddots & \ddots & \\ R_{5,1}(\bar{q}) & \cdots & R_{5,4}(\bar{q}) & I \end{bmatrix} \in \mathbb{R}^{10 \times 10}$$

Gravity term $\bar{\nu}(\bar{q})$ becomes equivalent to

$$\bar{\nu}(\bar{q}) = H^T L(\bar{q})^T M F(\bar{q})g_0 \tag{29}$$

where

$$F(\bar{q}) = \begin{bmatrix} R_{1,0}(\bar{q}) \\ \vdots \\ R_{5,0}(\bar{q}) \end{bmatrix} \in \mathbb{R}^{10 \times 2}$$

$$g_0^T = [\,0\ -g\,]$$

Input torque term $\bar{u}(\bar{q}, \dot{\bar{q}})$ is expressed as

$$\bar{u}(\bar{q}, \dot{\bar{q}}) = -P(\bar{q} - \hat{q}) - D(\dot{\bar{q}} - \dot{\hat{q}}) \tag{30}$$

where

$$P = \mathrm{diag}[\,0\ 0\ 0\ \kappa_2\ \cdots\ \kappa_5\,] \in \mathbb{R}^{7 \times 7}$$

$$D = \mathrm{diag}[\,0\ 0\ 0\ \sigma_2\ \cdots\ \sigma_5\,] \in \mathbb{R}^{7 \times 7}$$

and where $\hat{q}$ and $\dot{\hat{q}}$ are the desired states of $\bar{q}$ and $\dot{\bar{q}}$, respectively, and κ_i and σ_i $(i = 2, \ldots, 5)$ are gain constants.

During the swing phase, the tip of the stance leg is constrained on the ground. Therefore, we can set $x = 0$ and $y = 0$. Using Lagrange's undetermined multiplier, components of ground reaction force λ_x and λ_y $(\bar{\lambda} = [\,\lambda_x\ \lambda_y\ 0 \ldots 0\,]^T)$ are calculated from the first and second rows of (26). The equations of motion for state variables θ_i $(i = 1, \ldots, 5)$ are obtained from the other rows of (26), which equals (1).

When the swing leg touches the ground, an impulsive force acts on the leg tip. As described in Section 2.3, this results in discontinuous changes in the angular velocities. Following the derivation in [24] and assumptions FA1 through FA3 of the foot contact model described in Section 2.3, we integrate the equation of motion (26) from the start to the end of the double-supported phase to derive the relationship of the angular velocities. By considering the switching of the legs between swing and stance, velocity $\dot{q}^+$ immediately after foot contact is given as

$$\dot{q}^+ = \bar{S}_c\left\{I_{7\times7} - \bar{K}^{-1}\bar{E}_c^T\left(\bar{E}_c\bar{K}^{-1}\bar{E}_c^T\right)^{-1}\bar{E}_c\right\}\dot{\bar{q}}^-$$
$$= \bar{Q}(\bar{q}^-)\dot{\bar{q}}^- \tag{31}$$

where $\bar{K} = \bar{K}(\bar{q}^-)$, $\bar{E}_c = \bar{E}_c(\bar{q}^-)$, and

$$\bar{E}_c(\bar{q}) = \begin{bmatrix} I_{2\times2}\ R_{1,0}(\bar{q})^T\tilde{r}_1\ \ldots\ R_{5,0}(\bar{q})^T\tilde{r}_5 \end{bmatrix} H \in \mathbb{R}^{2 \times 7}$$

$$\bar{S}_c = \begin{bmatrix} O_{5\times2}\ S_c \end{bmatrix} \in \mathbb{R}^{5 \times 7}$$

Impulse ξ of this foot contact is given by

$$\xi = -\left(\bar{E}_\mathrm{C}\bar{K}^{-1}\bar{E}_\mathrm{C}^\mathrm{T}\right)^{-1}\bar{E}_\mathrm{C}\dot{\bar{q}}^-$$
$$= \bar{X}(\bar{q}^-)\dot{\bar{q}}^- \tag{32}$$

Note that, since the tip of the stance leg is constrained on the ground just before foot contact, $x^- = 0$, $y^- = 0$, $\dot{x}^- = 0$, and $\dot{y}^- = 0$. Therefore, we obtain (5) and (6), where

$$Q(q^-) = \bar{Q}(\bar{q}^-)\begin{bmatrix} O_{2\times 5} \\ I_{5\times 5} \end{bmatrix},\ X(q^-) = \bar{X}(\bar{q}^-)\begin{bmatrix} O_{2\times 5} \\ I_{5\times 5} \end{bmatrix} \tag{33}$$

B Angular momentum around the tip of the legs

In this appendix, we show the angular momentum around the tips of the legs, where the tip of the stance leg is constrained on the ground and $x = y = 0$. First, let $\bar{K}(\bar{q})\dot{\bar{q}} = [\ell_x(\bar{q},\dot{\bar{q}})\ \ell_y(\bar{q},\dot{\bar{q}})\ \ell_1(\bar{q},\dot{\bar{q}})\cdots\ell_5(\bar{q},\dot{\bar{q}})]^\mathrm{T}$ and $p(\bar{q},\dot{\bar{q}}) = [p_x(\bar{q},\dot{\bar{q}})\ p_y(\bar{q},\dot{\bar{q}})\ p_1(\bar{q},\dot{\bar{q}})\cdots p_5(\bar{q},\dot{\bar{q}})]^\mathrm{T}$. Angular momentum $\ell_\mathrm{sw}(\bar{q},\dot{\bar{q}})$ around the tip of the swing leg is then given as

$$\ell_\mathrm{sw}(\bar{q},\dot{\bar{q}}) = \ell_1(\bar{q},\dot{\bar{q}}) - \tilde{r}_\mathrm{sw}(\bar{q})^\mathrm{T} p_1(\bar{q},\dot{\bar{q}}) \tag{34}$$

where

$$r_\mathrm{sw}(\bar{q}) = r_1 + \sum_{i=2}^{5} R_{i,1}(\bar{q})^\mathrm{T} r_i$$

In contrast, angular momentum $\ell_\mathrm{st}(\bar{q},\dot{\bar{q}})$ around the tip of the stance leg becomes

$$\ell_\mathrm{st}(\bar{q},\dot{\bar{q}}) = \ell_1(\bar{q},\dot{\bar{q}}) \tag{35}$$

C Derivation of the Jacobian matrix of the Poincaré map

In this appendix, we derive the Jacobian matrix of a Poincaré map based on an approximate analysis to investigate local stability (for a detailed derivation, see [4,6,13], for example). Note that the derivation is performed by incorporating all of the perturbations for the state variables without confining these perturbations in the Poincaré section.

First, the relationship between the states just before and after foot contact (16) yields

$$B = \partial_q h(q^*(\tau))$$
$$= \begin{bmatrix} 1 & 0 & -2\cos\phi_0 & 2s\sin\phi_0 \\ 0 & 1 & B_{23} & B_{24} \\ 0 & 0 & 1 & 0 \\ 0 & 0 & 0 & 1 \end{bmatrix} \tag{36}$$

where $\partial_q = \frac{\partial}{\partial q}$ and

$$B_{23} = 2\omega(\alpha_3+\alpha_4)(2\kappa s^2\cos\phi_0 + \sin\phi_0)/\alpha_1$$
$$B_{24} = s\omega\{2(\alpha_3+\alpha_4)\cos\phi_0 - \alpha_5\alpha^2\beta\}/\alpha_1$$

Second, the geometric condition for foot contact (14) yields

$$D = I_{4\times 4} - \frac{\dot{q}^*(\tau)\partial_q r(q^*(\tau))^\mathrm{T}}{\partial_q r(q^*(\tau))^\mathrm{T}\dot{q}^*(\tau)}$$
$$= \frac{1}{D_0}\begin{bmatrix} s\omega\sin\phi_0 & 0 & \dot{\theta}_1^*(\tau)\cos\phi_0 & -\dot{\theta}_1^*(\tau)s\sin\phi_0 \\ -\ddot{\theta}_1^*(\tau) & D_0 & \ddot{\theta}_1^*(\tau)\cos\phi_0 & -\ddot{\theta}_1^*(\tau)s\sin\phi_0 \\ 0 & 0 & D_0 & 0 \\ -\omega & 0 & \omega\cos\phi_0 & \dot{\theta}_1^*(\tau) \end{bmatrix} \tag{37}$$

where

$$\dot{\theta}_1^*(\tau) = -(k_2+k_3)\lambda\{\cosh(\lambda t_0) - 1\}/\sinh(\lambda\tau) + k_1\omega\sin\phi_0$$
$$\qquad +(s+k_1)\lambda\cos\phi_0\cosh(\lambda\tau/2)/\sinh(\lambda\tau/2)$$
$$\ddot{\theta}_1^*(\tau) = \{s\lambda^2 + k_1(\lambda^2+\omega^2)\}\cos\phi_0$$
$$\quad D_0 = \dot{\theta}_1^*(\tau) + s\omega\sin\phi_0$$

Third, by integrating the following equation from $t = 0$ to $t = \tau$

$$\delta\dot{q}(t) = \partial_q f(q^*(t))\delta q(t) \tag{38}$$

where δq is the perturbation, we obtain

$$E = \begin{bmatrix} \cosh(\lambda\tau) & \sinh(\lambda\tau)/\lambda & E_{13} & E_{14} \\ \lambda\cosh(\lambda\tau) & \cosh(\lambda\tau) & E_{23} & E_{24} \\ 0 & 0 & e^{-2\kappa\omega s^2\tau} & 0 \\ 0 & 0 & 0 & 1 \end{bmatrix} \tag{39}$$

where

$$E_{13} = \{[\cosh(\lambda\tau) + e^{-2\kappa\omega s^2\tau} - 2\kappa\omega s^2\sinh(\lambda\tau)/\lambda](\epsilon_1\eta_1 + \epsilon_2\eta_2)$$
$$\quad -\sinh(\lambda\tau)\omega(\epsilon_1\eta_2 - \epsilon_2\eta_1)/\lambda + \{\cosh(\lambda\tau) - \cosh(\lambda\Delta)e^{-2\kappa\omega s^2 t_0}$$
$$\quad -2\kappa\omega s^2[\sinh(\lambda\tau) - \sinh(\lambda\Delta)e^{-2\kappa\omega s^2 t_0}]/\lambda\}(\epsilon_3 d_1 + \epsilon_4 d_2 + \epsilon_5)$$
$$\quad -\{\sinh(\lambda\tau) - \sinh(\lambda\Delta)e^{-2\kappa\omega s^2 t_0}\}\alpha\omega(\epsilon_3 d_2 - \epsilon_4 d_1)/\lambda$$
$$E_{23} = \{\lambda\sinh(\lambda\tau) - 2\kappa\omega s^2[e^{-2\kappa\omega s^2\tau} + \cosh(\lambda\tau)]\}(\epsilon_1\eta_1 + \epsilon_2\eta_2)$$
$$\quad -\{\cosh(\lambda\tau) + e^{-2\kappa\omega s^2\tau}\}\omega(\epsilon_1\eta_2 - \epsilon_2\eta_1)$$
$$\quad +\{\lambda[\sinh(\lambda\tau) - \sinh(\lambda\Delta)e^{-2\kappa\omega s^2 t_0}] - 2\kappa\omega s^2[\cosh(\lambda\tau)$$
$$\quad -\cosh(\lambda\Delta)e^{-2\kappa\omega s^2 t_0}]\}(\epsilon_3 d_1 + \epsilon_4 d_2 + \epsilon_5)$$
$$\quad -\{\cosh(\lambda\tau) - \cosh(\lambda\Delta)e^{-2\kappa\omega s^2 t_0}\}\alpha\omega(\epsilon_3 d_2 - \epsilon_4 d_1)$$
$$E_{14} = \epsilon_6\{[\cosh(\lambda\tau) + 1]\sin\phi_0 + \sinh(\lambda\tau)\omega\cos\phi_0/\lambda\}$$
$$\quad +\epsilon_7\{\sinh(\lambda\tau) - \sinh(\lambda\Delta)\}/\lambda$$
$$E_{24} = \epsilon_6\{\lambda\sinh(\lambda\tau)\sin\phi_0 + [\cosh(\lambda\tau) + 1]\omega\cos\phi_0\}$$
$$\quad +\epsilon_7\{\cosh(\lambda\tau) - \cosh(\lambda\Delta)\}$$
$$\epsilon_1 = \{\omega^2(\alpha_3+\alpha_4)(4\kappa^2 s^4 - 1) - (\beta_3+\beta_4)\}/\{\alpha_1(c_1^2 + c_2^2)\}$$
$$\epsilon_2 = (\alpha_3+\alpha_4)4\kappa\omega^2 s^2/\{\alpha_1(c_1^2 + c_2^2)\}$$
$$\epsilon_3 = \beta\{-\alpha_5\omega^2(4\kappa^2 s^4 - \alpha^2) + \beta_5\}/\{\alpha_1(d_1^2 + d_2^2)\}$$
$$\epsilon_4 = -4\beta\alpha_5\kappa\omega^2 s^2\alpha/\{\alpha_1(d_1^2 + d_2^2)\}$$
$$\epsilon_5 = \beta(4\alpha_5\kappa^2\omega^2 s^4 - \beta_5)/\{\alpha_1(4\kappa^2\omega^2 s^4 - \lambda^2)\}$$
$$\epsilon_6 = -s\{(\alpha_3+\alpha_4)\omega^2 + \beta_3 + \beta_4\}/\{\alpha_1(\omega^2+\lambda^2)\}$$
$$\epsilon_7 = s\alpha^2\omega\beta(\alpha_5\alpha^2\omega^2 + \beta_5)/\{\alpha_1(\omega^2+\lambda^2)\}$$
$$\eta_1 = c_1\cos\phi_0 - c_2\sin\phi_0,\ \eta_2 = c_1\sin\phi_0 + c_2\cos\phi_0$$
$$c_1 = 4\kappa^2\omega^2 s^4 - \omega^2 - \lambda^2,\ c_2 = 4\kappa^2\omega^2 s^2$$
$$d_1 = 4\kappa^2\omega^2 s^4 - \alpha^2\omega^2 - \lambda^2,\ d_2 = 4\kappa^2\omega^2 s^2\alpha$$

From matrices B, D, and E, Jacobian matrix $\mathcal{J}$ of the Poincaré map is obtained by $\mathcal{J} = BDE$, which is equivalent (19).

When we incorporate phase resetting, matrix B becomes $\tilde{B}$, which is given as

$$\tilde{B} = \partial_q \tilde{h}(q^*(\tau))$$
$$= \begin{bmatrix} 1 & 0 & -2\cos\phi_0 & 2s\sin\phi_0 \\ 0 & 1 & \tilde{B}_{23} & \tilde{B}_{24} \\ 0 & 0 & 1 & -s\tan\phi_0 \\ 0 & 0 & 0 & 0 \end{bmatrix} \tag{40}$$

where

$$\tilde{B}_{23} = B_{23}$$
$$\tilde{B}_{24} = -s\omega(\alpha_3+\alpha_4)(2\kappa s^2\sin\phi_0 + \sin\phi_0\tan\phi_0 - \cos\phi_0)/\alpha_1$$

In this case, Jacobian matrix $\tilde{\mathcal{J}}$ of the Poincaré map is calculated by $\tilde{\mathcal{J}} = \tilde{B}DE$, resulting in (24).

References

1. R. Altendorfer, N. Moore, H. Komsuoglu, M. Buehler, H.B. Brown Jr., D. McMordie, U. Saranli, R. Full, and D.E. Koditschek, *RHex: A biologically inspired hexapod runner*, Auton. Robots, 11(3):207–213, 2001.

2. S. Aoi and K. Tsuchiya, *Locomotion control of a biped robot using nonlinear oscillators*, Auton. Robots, 19(3):219–232, 2005.

3. S. Aoi and K. Tsuchiya, *Adaptive behavior in turning of an oscillator-driven biped robot*, Auton. Robots, 23(1):37–57, 2007.

4. S. Aoi and K. Tsuchiya, *Self-stability of a simple walking model driven by a rhythmic signal*, Nonlinear Dyn., 48(1-2):1–16, 2007.

5. S. Aoi and K. Tsuchiya, *Bifurcation and chaos of a simple walking model driven by a rhythmic signal*, Int. J. Non-Linear Mech., 41(3): 438–446, 2006.

6. S. Aoi and K. Tsuchiya, *Stability analysis of a simple walking model driven by an oscillator with a phase reset using sensory feedback*, IEEE Trans. Robotics, 22(2):391–397, 2006.

7. S. Aoi, H. Sasaki, and K. Tsuchiya, *A multilegged modular robot that meanders: Investigation of turning maneuvers using its inherent dynamic characteristics*, SIAM J. Appl. Dyn. Syst., 6(2):348-377, 2007.

8. S. Aoi, N. Ogihara, Y. Sugimoto, and K. Tsuchiya, *Simulating adaptive human bipedal locomotion based on phase resetting using foot-contact information*, Adv. Robot., 22(15):1697-1713, 2008.

9. S. Aoi, N. Ogihara, T. Funato, Y. Sugimoto, and K. Tsuchiya, *Evaluating functional roles of phase resetting in generation of adaptive human bipedal walking with a physiologically based model of the spinal pattern generator*, Biol. Cybern., 102(5):373-387, 2010.

10. F. Asano and M. Yamakita, *Virtual gravity and coupling control for robotic gait synthesis*, IEEE Trans. Syst., Man, Cybern. Part A, 31(6):737–745, 2001.

11. R.E. Burke, A.M. Degtyarenko, and E.S. Simon, *Patterns of locomotor drive to motoneurons and last-order interneurons: Clues to the structure of the CPG*, J. Neurophysiol., 86:447-462, 2001.

12. J.G. Cham, J.K. Karpick, and M.R. Cutkosky, *Stride period adaptation of a biomimetic running hexapod*, Int. J. Robotics Res., 23(2):141–153, 2004.

13. M. Coleman, A. Chatterjee, and A. Ruina, *Motions of a rimless spoked wheel: A simple three-dimensional system with impacts*, Dynam. Stabil. Syst., 12(3):139–160, 1997.

14. J.J. Collins and I.N. Stewart, *Coupled nonlinear oscillators and the symmetries of animal gaits*, J. Nonlinear Sci., 3:349–392, 1993.

15. S.H. Collins, A.L. Ruina, R. Tedrake, and M. Wisse, *Efficient bipedal robots based on passive-dynamic walkers*, Science, 307:1082–1085, 2005.

16. G. Courtine and M. Schieppati, *Human walking along a curved path. II. Gait features and EMG patterns*, Eur. J. Neurosci., 18(1):191–205, 2003.

17. A.C. de Pina Filho, M.S. Dutra, L.S.C. Raptopoulos, *Modeling of a bipedal robot using mutually coupled Rayleigh oscillators*, Biol. Cybern., 92:1–7, 2005.

18. M.S. Dutra, A.C. de Pina Filho, and V.F. Romano, *Modeling of a bipedal locomotor using coupled nonlinear oscillators of Van der Pol*, Biol. Cybern., 88:286–292, 2003.

19. Y. Fukuoka, H. Kimura, and A. Cohen, *Adaptive dynamic walking of a quadruped robot on irregular terrain based on biological concepts*, Int. J. Robotics Res., 22(3-4):187–202, 2003.

20. M. Garcia, A. Chatterjee, A. Ruina, and M. Coleman, *The simplest walking model: Stability, complexity, and scaling*, ASME J. Biomech. Eng., 120(2):281–288, 1998.

21. A. Goswami, B. Espiau, and A. Keramane, *Limit cycles in a passive compass gait biped and passivity-mimicking control laws*, Auton. Robots, 4:273–286, 1997.

22. S. Grillner, *Control of locomotion in bipeds, tetrapods and fish*, Handbook of Physiology, American Physiological Society, Bethesda, MD, pp. 1179–1236, 1981.

23. S. Grillner, *Neurobiological bases of rhythmic motor acts in vertebrates*, Science, 228:143–149, 1985.

24. J.W. Grizzle, G. Abba, and F. Plestan, *Asymptotically stable walking for biped robots: Analysis via systems with impulse effects*, IEEE Trans. Autom. Control, 46(1):51–64, 2001.

25. K. Hirai, M. Hirose, Y. Haikawa, and T. Takenaka, *The development of the Honda humanoid robot*, In Proc. IEEE Int. Conf. on Robot. Autom., pp. 1321–1326, 1998.

26. K. Hosoda, T. Takuma, A. Nakamoto, and S. Hayashi, *Biped robot design powered by antagonistic pneumatic actuators for multi-modal locomotion*, Robot. Auton. Syst., 56(1): 46–53, 2008.

27. A.J. Ijspeert, A. Crespi, D. Ryczko, and J.M. Cabelguen, *From swimming to walking with a salamander robot driven by a spinal cord model*, Science, 315:1416–1420, 2007.

28. A.J. Ijspeert, *Central pattern generators for locomotion control in animals and robots: a review*, Neural Netw., 21(4):642–653, 2008.

29. S. Inagaki, H. Yuasa, and T. Arai, *CPG model for autonomous decentralized multi-legged robot system–generation and transition of oscillation patterns and dynamics of oscillators*, Robot. Auton. Syst., 44(3-4):171–179, 2003.

30. K. Inoue, S. Ma, and C. Jin, *Neural oscillator network-based controller for meandering locomotion of snake-like robots*, In Proc. IEEE Int. Conf. on Robot. Autom., pp. 5064–5069, 2004.

31. K. Kaneko, F. Kanehiro, S. Kajita, H. Hirukawa, T. Kawasaki, M. Hirata, K. Akachi, and T. Isozumi, *Humanoid robot HRP-2*, In Proc. IEEE Int. Conf. on Robot. Autom., pp. 1083–1090, 2004.

32. R. Katoh and M. Mori, *Control method of biped locomotion giving asymptotic stability of trajectory*, Automatica, 20(4):405–414, 1984.

33. H. Kimura, Y. Fukuoka, and A. Cohen, *Adaptive dynamic walking of a quadruped robot on natural ground based on biological concepts*, Int. J. Robotics Res., 26(5):475–490, 2007.

34. A.D. Kuo, *Energetics of actively powered locomotion using the simplest walking model*, ASME J. Biomech. Eng., 124:113–120, 2002.

35. Y. Kuroki, M. Fujita, T. Ishida, K. Nagasaka, and J. Yamaguchi, *A small biped entertainment robot exploring attractive applications*, In Proc. IEEE Int. Conf. on Robot. Autom., pp. 471–476, 2003.

36. M.A. Lewis and G.A. Bekey, *Gait adaptation in a quadruped robot*, Auton. Robots, 12(3):301–312, 2002.

37. M.A. Lewis, R. Etienne-Cummings, M.J. Hartmann, Z.R. Xu, and A.H. Cohen, *An in silico central pattern generator: silicon oscillator, coupling, entrainment, and physical computation*, Biol. Cybern., 88:137–151, 2003.

38. K. Löffler, M. Gienger, and F. Pfeiffer, *Sensors and control concept of walking "Johnnie"*, Int. J. Robotics Res., 22(3-4):229–239, 2003.

39. T. McGeer, *Passive dynamic walking*, Int. J. Robotics Res., 9(2):62–82, 1990.

40. J. Nakanishi, J. Morimoto, G. Endo, G. Cheng, S. Schaal, and M. Kawato, *Learning from demonstration and adaptation of biped locomotion*, Robot. Auton. Syst., 47(2-3):79–91, 2004.

41. M. Nakanishi, T. Nomura, and S. Sato, *Stumbling with optimal phase reset during gait can prevent a humanoid from falling*, Biol. Cybern., 95:503–515, 2006.

42. K. Nishiwaki, T. Sugihara, S. Kagami, F. Kanehiro, M. Inaba, and H. Inoue, *Design and development of research platform for perception-action integration in humanoid robot: H6*, In Proc. IEEE/RSJ Int. Conf. on Intell. Robots Syst., pp. 1559–1564, 2000.

43. G.N. Orlovsky, T. Deliagina, and S. Grillner, *Neuronal control of locomotion: from mollusc to man*, Oxford University Press, 1999.

44. A.E. Patla, T.W. Calvert, and R.B. Stein, *Model of a pattern generator for locomotion in mammals*, Am. J. Physiol. Reg. Integ. Comp. Physiol. 248:484-494, 1985.

45. I. Poulakakis, J.A. Smith, and M. Buehler, *Modeling and experiments of untethered quadrupedal running with a bounding gait: The Scout II Robot*, Int. J. Robotics Res., 24(4):239–256, 2005.

46. R.D. Quinn, G.M. Nelson, R.J. Bachmann, D.A. Kingsley, J.T. Offi, T.J. Allen, and R.E. Ritzmann, *Parallel complementary strategies for implementing biological principles into mobile robots*, Int. J. Robotics Res., 22(3):169–186, 2003.

47. L. Righetti and A.J. Ijspeert, *Programmable central pattern generators: an application to biped locomotion control*, In Proc. IEEE Int. Conf. on Robot. Autom., pp. 1585–1590, 2006.

48. I.A. Rybak, K. Stecina, N.A. Shevtsova, and D.A. McCrea, *Modelling spinal circuitry involved in locomotor pattern generation: insights from the effects of afferent stimulation*, J. Physiol., 577(2):641-658, 2006.

49. U. Saranli, M. Buehler, and D.E. Koditschek, *RHex: A simple and highly mobile hexapod robot*, Int. J. Robotics Res., 20(7):616–631, 2001.

50. G. Schtner, W.Y. Jiang, J.A.S. Kelso, *A synergetic theory of quadrupedal gaits and gait transitions*, J. Theor. Biol. 142:359-391, 1990.

51. G. Taga, Y. Yamaguchi, and H. Shimizu, *Self-organized control of bipedal locomotion by neural oscillators in unpredictable environment*, Biol. Cybern., 65:147–159, 1991.

52. G. Taga, *A model of the neuro-musculo-skeletal system for human locomotion I. Emergence of basic gait*, Biol. Cybern., 73:97–111, 1995.

53. G. Taga, *A model of the neuro-musculo-skeletal system for human locomotion II. - Real-time adaptability under various constraints*, Biol. Cybern., 73:113–121, 1995.

54. T. Takuma and K. Hosoda, *Controlling the walking period of a pneumatic muscle walker*, Int. J. Robotics Res., 25(9): 861–866, 2006.

55. K. Tsujita, K. Tsuchiya, and A. Onat, *Adaptive gait pattern control of a quadruped locomotion robot*, In Proc. IEEE/RSJ Int. Conf. on Intell. Robots Syst., pp. 2318–2325, 2001.

56. M. Vukobratović, B. Borovac, D. Surla, and D. Stokić, *Biped locomotion-dynamics, stability, control and application*, Springer-Verlag, 1990.

57. E.R. Westervelt, J.W. Grizzle, and D.E. Koditschek, *Hybrid zero dynamics of planar biped walkers*, IEEE Trans. Autom. Control, 48(1):42–56, 2003.

58. D.A. Winter, *Biomechanics and motor control of human movement (3rd edition)*, New York: John Wiley & Sons, 2004.

59. M. Wisse, A.L. Schwab, R.Q. van der Linde, and F.C.T. van der Helm, *How to keep from falling forward: elementary swing leg action for passive dynamic walkers*, IEEE Trans. Robotics, 21(3):393–401, 2005.

60. J. Yamaguchi, E. Soga, S. Inoue, and A. Takanishi, *Development of a bipedal humanoid robot - Control method of whole body cooperative dynamic biped walking -*, In Proc. IEEE Int. Conf. on Robot. Autom., pp. 368–374, 1999.

61. T. Yamasaki, T. Nomura, and S. Sato, *Possible functional roles of phase resetting during walking*, Biol. Cybern., 88:468–496, 2003.

62. M. Yano, S. Hibiya, M. Tokiwa, and Y. Makino, *Real-time control of walking of insect; Self-organization of the constraints and walking patterns*, Distributed Autonomous Robotic System 5, H. Asama, T. Arai, T. Fukuda, and T. Hasegawa (Eds.), Springer-Verlag, Tokyo, pp. 444-451, 2002.

63. H. Yuasa and M. Ito, *Coordination of many oscillators and generation of locomotory patterns*, Biol. Cybern., 63:177-184, 1990.

64. T. Zielinska, *Coupled oscillators utilised as gait rhythm generators of a two-legged walking machine*, Biol. Cybern., 74:263–273, 1996.